Probing the Effect of the Non-Active-Site Mutation Y229W in New Delhi Metallo-β-lactamase-1 by Site-Directed Mutagenesis, Kinetic Studies, and Molecular Dynamics Simulations

Jiao Chen[◑], Hui Chen[◑], Yun Shi, Feng Hu, Xingzhen Lao, Xiangdong Gao, Heng Zheng*, Wenbing Yao*

School of Life Science and Technology, China Pharmaceutical University, Nanjing, Jiangsu, China

Abstract

New Delhi metallo-β-lactmase-1 (NDM-1) has attracted extensive attention for its high catalytic activities of hydrolyzing almost all β-lactam antibiotics. NDM-1 shows relatively higher similarity to subclass B1 metallo-β-lactmases (MβLs), but its residue at position 229 is identical to that of B2/B3 MβLs, which is a Tyr instead of a B1-MβL-conserved Trp. To elucidate the possible role of Y229 in the bioactivity of NDM-1, we performed mutagenesis study and molecular dynamics (MD) simulations. Although residue Y229 is spatially distant from the active site and not contacting directly with the substrate or zinc ions, the Y229W mutant was found to have higher k_{cat} and K_m values than those of wild-type NDM-1, resulting in 1~7 fold increases in k_{cat}/K_m values against tested antibiotics. In addition, our MD simulations illustrated the enhanced flexibility of Loop 2 upon Y229W mutation, which could increase the kinetics of both substrate entrance (kon) and product egress (koff). The enhanced flexibility of Loop 2 might allow the enzyme to adjust the geometry of its active site to accommodate substrates with different structures, broadening its substrate spectrum. This study indicated the possible role of the residue at position 229 in the evolution of NDM-1.

Competing Interests: The authors have declared that no competing interests exist.

* E-mail: zhengh18@hotmail.com (HZ); wbyao@cpu.edu.cn(WY)

[◑] These authors contributed equally to this work.

Introduction

Metallo-β-lactamases (MβLs) caused antibiotic resistance has become a main therapeutic challenge in the clinic [1]. These enzymes are characterized by one or two zinc ions that are indispensable for enzyme activities [2]. The zinc ions in the active site activate a coordinated water molecule, forming a hydroxide moiety that acts as a nucleophile to attack the carbonyl group within the β-lactam ring [3]. MβLs have raised major concerns due to their broad hydrolytic spectrum on β-lactams and the absence of effective inhibitors for clinical treatment [4].

New Delhi metallo-β-lactamase (NDM-1) was first identified from *Klebsiella pneumonia*, isolated from a Swedish patient who had travelled to New Delhi [5]. NDM-1-positive strains can degrade almost all β-lactam antibiotics, including penicillins, cephalosporins, and the highly potent carbapenems [6]. NDM-1 genes are encoded on plasmids, facilitating their transmission across different bacterial strains. In addition, the widespread use of β-lactams has created selective pressure that promotes the dissemination of MβLs genes. Consequently, NDM-1 has spread to nearly every continent worldwide after its first identification and has become a formidable threat to human health [7].

Based on their amino acid sequences and zinc ion dependence, MβLs have been divided into subclasses B1, B2, and B3, all of which share a similar αβ/βα scaffold [8]. The subclass B1 enzymes have emerged as the most clinically significant MβLs with two zinc ions in the active site [9]. NDM-1 is grouped into subclass B1 and has been investigated by several structural studies [10–12]. The functional significance of several residues in the active site has been studied, including D124 (NDM-1 numbering is used throughout the paper, unless otherwise specified), which plays a critical role in the catalytic reaction with its exact function remains controversial [13]. Nevertheless, there have been relatively few studies on the role of non-active-site residues. The rapid evolution of NDM MβLs figured out that non-active-site residue mutations can also influence the activity of NDM-1. Two recent studies showed the increased hydrolytic activities of NDM-4 and NDM-5, which differ from NDM-1 by non-active-site amino acid substitutions (M154L for NDM-4, V88L and M154L for NDM-5), toward carbapenems and several cephalosporins [14,15].

Y229, which is structurally distant from the active site and not in direct contact with the substrate or zinc ions, has been shown to be an interesting residue in NDM-1 [12]. In subclass B1 MβLs, a Trp (W) residue is conserved at position 229 (position 244 in BBL numbering system [16], while in subclass B2 and B3 MβLs, it is a

Tyr (Y) residue at this position (Fig. 1). Hence, NDM-1 is a remarkable exception in subclass B1, with a Tyr residue at position 229 that parallels subclass B2/B3 MβLs. It is reported that B2 (e.g. CphA, Sfh-1) and B3 (e.g. FEZ, L1) MβLs present narrower substrate spectrum than NDM-1 [6,8,17]. In order to probe the role of Y229 on the structure and activity of MβLs, we constructed the Y229W mutant of NDM-1 by site-directed mutagenesis and studied its kinetic properties. Molecular dynamics simulations have also been conducted to examine the structural changes upon mutation.

Materials and Methods

Site-directed mutagenesis and enzymatic activity assay

Construction of NDM-1 and Y229W mutant. The wild-type NDM-1 gene lacking the signal peptide was synthesized chemically and then cloned between EcoRI and Hind III restriction sites into the pET-28a plasmid harboring a kanamycin resistance gene. This bla_{NDM-1}-encoding plasmid was used to introduce Y229W mutation by site-directed mutagenesis. The forward primer was 5′-GACACTGAGCACTGGGCCGCGT-CAGC-3′ and the reverse primer was 5′-GCTGACGCGGCC-CAGTGCTCAGTGTC-3′. The mutated gene was cloned between the same restriction sites into pET-28a as wild-type NDM-1.

The constructed plasmids encoding wild-type NDM-1 and Y229W mutant were transferred into E.coli BL21 (DE3). The enzymes were expressed and purified as previously described [18]. The N-terminal 6×His-Tag was removed by thrombin catalysis, followed by Ni column purification.

Determination of kinetic parameters. Hydrolysis of the antibiotics by wild-type NDM-1 and Y229W mutant was monitored by following the absorbance variation that resulted from the opening of the β-lactam ring [19]. All the measurements were performed at 30°C in the buffer of 50 mM HEPES, 250 mM NaCl, 200 μM ZnCl₂, and pH = 7.25, using a UV-1800 spectrophotometer (Mapada, Shanghai, China). The molar extinction coefficients and wavelengths used in the assays were referred to those from [20,21]. The steady-state kinetic parameters (K_m and k_{cat}) were determined at least three times by fitting the concentration dependence of initial rate measurements to the Michaelis-Menten equation.

Determination of minimum inhibitory concentrations (MICs). MICs for E.coli BL21 (DE3) harboring NDM-1 and Y229W mutant were determined by a two-fold serial dilution method on 96-well microplates. E.coli BL21 (DE3)/pET-28a was used as negative control. The bacteria were diluted to 1×10^6 CFU/ml by Luria-Bertani (LB) broth containing 50 μg/ml kanamycin and then incubated at 37°C for 12 hours after adding different concentrations of antibiotics. A reading at 600 nm was taken to determine the MICs.

Molecular dynamics analysis of NDM-1 and Y229W mutant

Initial model building. Molecular dynamics (MD) simulations were employed to investigate the dynamic properties of NDM-1 and the Y229W mutant with/without the hydrolyzed Ampicillin (PDB entry: 3Q6X). The structure of Y229W mutant was built in Discovery Studio 2.5.5. Prior to modeling, all crystal waters were removed except for the bridging water, which was assumed to exist in hydroxide form between the two zinc ions. The bridging water was thus parameterized as a hydroxide ion in the MD simulations of the apo-enzyme (without substrate) and was deleted in enzyme-substrate systems.

Zinc ions were modeled as "cationic dummy atoms" (CaDA), which allowed for modeling of the binuclear Zn-containing proteins without having to covalently attach the coordinating residues to the Zn atoms. In this approach, the zinc's vacant $4s4p^3$ orbitals that accepted electron density of the four ligands were modeled by four identical dummy atoms, which were covalently bonded to the zinc nucleus and carried a partial charge of +0.5e each [22]. These dummy atoms have been shown to keep the ligands in the correct orientation, which enables a stable simulation of the tetrahedral coordination of the zinc atoms in IMP metallo-β-lactamases [23,24].

In our model, zinc-coordinating histidines 120, 122, 189 and 250 were treated as histidinates, while Cys208 was assumed to be deprotonated at the S_γ position. Atom charges of the substrate were calculated using the RESP method [25] encoded in the AMBER 12.0 software package [26] at the HF/6-31G* level. As a comparison, the wild-type NDM-1 (PDB entry 3Q6X) was
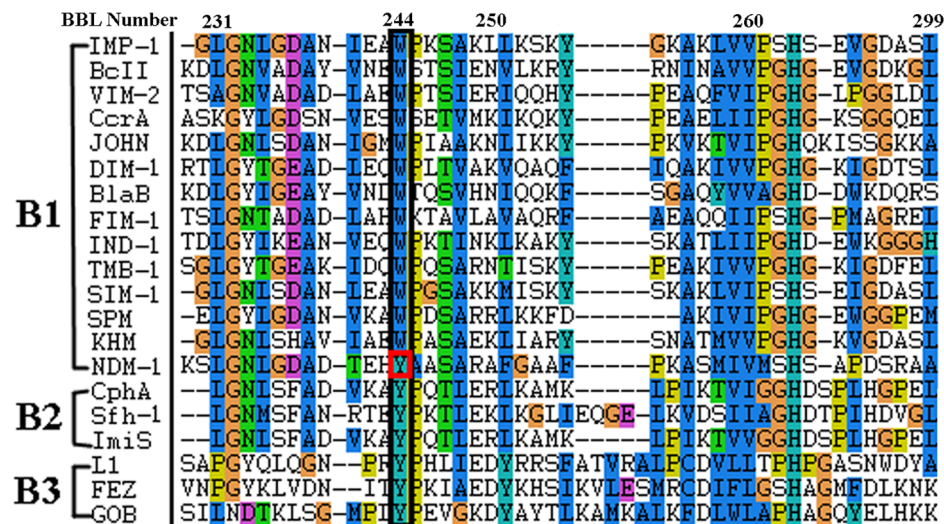

Figure 1. The sequence alignment of MβLs around position 244 (BBL number), parallel with position 229 in NDM-1.
doi:10.1371/journal.pone.0082080.g001

modeled with the same method as the Y229W mutant. Zinc dummy atoms were created using zinc, histidinate and hydroxide force field parameters provided by [22].

Molecular dynamics. Molecular dynamics simulations were performed with AMBER12.0. Each model was solvated in a periodic box of TIP3P [27] water molecules that extend 10 Å from the protein atoms. Counter-ions were added to neutralize the simulation systems. The ff12SB force field was used for the protein systems. To remove possible poor contacts between the solute and solvent, energy minimization (1000 steps for the water molecules followed by 3000 steps for the whole system) were performed before MD simulations. The SANDER program included in AMBER 12.0 was used to conduct the MD simulations at constant temperature and pressure with a time step of 1 fs. The temperature (300 K) and pressure (1.0 atm) of the system was controlled by the Langevin algorithm [28]. Electrostatic interactions were calculated using the particle-mesh Ewald method [29], and the non-bonded cutoff was set to 10.0 Å. The SHAKE algorithm [30] was used to constrain bonds involving hydrogen atoms. Each system was equilibrated for 500 ps under a NPT ensemble at a constant temperature of 300 K. Following this equilibration, production MD simulations were conducted for 20 ns for all systems with a time step of 1 fs.

Analysis of simulations. The ptraj analysis program within AMBER 12.0 was used for the calculations of the root mean square deviation (RMSD), the root mean square fluctuation (RMSF) and the existence of hydrogen bonds.

Based on the equilibrated dynamics trajectory (the last 4ns), the binding free energy of each complex system was calculated using the MMPBSA.py module. A total of 400 snapshots from the trajectory were extracted every 20 ps, and the MM/PBSA and MM/GBSA calculations were performed on each snapshot. The binding free energies (ΔG) were computed according to the following equations [31]:

$$\Delta G = <\Delta G_{gas}> + <\Delta G_{solv}> - <T\Delta S> \qquad (1)$$

$$\Delta G_{gas} = \Delta G_{elec} + \Delta G_{vdW} + \Delta G_{int} \qquad (2)$$

$$\Delta G_{sol} = \Delta G_{PB/GB} + \Delta G_{np} \qquad (3)$$

$$\Delta G_{np} = \gamma \times SASA + \beta \qquad (4)$$

where $<...>$ indicates an average of an energy term along the MD simulation trajectory. ΔG_{gas} and ΔG_{solv} represent the vacuum and solvation binding free energies, respectively. $-T\Delta S$ is the entropic contribution, which is not considered in the relative free energy analysis. ΔG_{gas} includes an intermolecular electrostatic term (ΔG_{elec}), a van der Waals term (ΔG_{vdW}), and an internal energy term (ΔG_{int}). ΔG_{solv} is divided into the electrostatic solvation energy ($\Delta G_{PB/GB}$) and the nonpolar solvation energy (ΔG_{np}). γ is the surface tension proportionality constant and β is the offset value. The solvent accessible surface area (SASA) was estimated by the MSMS algorithm with a probe radius of 1.4 Å [32].

Results

Experimental results

Kinetic parameters. Steady state kinetic parameters of wild-type NDM-1 and Y229W mutant with different antibiotics are summarized in Table 1. The K_m values of Y229W mutant increased 1.5–5 times compared with wild-type NDM-1, while the catalytic constant k_{cat} showed greater increases of 12–25 times against Penicillin G, Cefuroxime, Ceftizoxime and Meropenem. Thus, their increases in the hydrolytic efficiency (3∼7 folds) upon Y229W mutation was mainly due to the increase in the turnover rate rather than binding affinities. Specifically, the k_{cat} of Penicillin G showed the largest increase after Y229W mutation, from 34 ± 1.5 s^{-1} to 849 ± 28 s^{-1}, resulting in a 6 fold increase in k_{cat}/K_m. For Ampicillin, the Y229W mutant showed similar K_m and k_{cat} values to those of wild-type NDM-1, and no significant change was observed in k_{cat}/K_m.

Antibiotic susceptibility tests. To determine the antibiotic susceptibility of Y229W mutant and wild-type NDM-1, the MICs of Penicillin G, Ampicillin, Cefuroxime, Ceftizoxime and Meropenem were measured (Table 2). The *E.coli* BL21 harboring Y229W mutant showed strong resistance to Penicillin G, yielding a MIC of 256 μg/ml. The MICs of Ampicillin, Cefuroxime, and Meropenem decreased at least two folds after mutation, whereas a 8 fold decrease was observed in the case of Ceftizoxime. Therefore, the Y229W mutant rendered the host strain more susceptible to all tested antibiotics.

Molecular dynamics

Overview of the structure around Y229. The active site of NDM-1 is located at the bottom of a shallow groove enclosed by two important loops, namely Loop 1 and Loop 2. The role of Loop 1 and the N-terminal of Loop 2 has been investigated by both experimental and computational methods [33,34]. The flexibility presumably assists in the structural rearrangement of the active site during catalytic turnover, granting interactions with a variety of substrates in B1 metallo-β-lactamases. Residing at the N-terminal of the helix α1, Y229 may play an important role in controlling the stability and flexibility of Loop 2, as it can form extensive hydrophobic interactions with neighboring residues, including L209, L218, and L221 in Loop 2, and L269 in helix α2 (Fig. 2). In addition, a hydrogen bond is also formed between the phenolic hydroxyl of Y229 and the backbone oxygen of residue L209. To investigate the role of the residue at 229 in the evolution of enzymatic activity, Y229 was selected to be mutated to Trp.

Dynamics and flexibility of the enzymes. The root-mean-square deviation (RMSD) values of wild-type NDM-1 and Y229W mutant against the starting structures were calculated. The RMSDs of backbone atoms stabilized after 11 ns of simulation for NDM-1 and 15 ns for the Y229W mutant system, indicating that the Y229W mutant underwent a larger conformational change to reach equilibrium (Fig. 3C). The stabilized RMSD

Table 1. Kinetic parameters of the wild-type NDM-1 and the Y229W mutant.

Antibiotics	Wild-type NDM-1			Y229W mutant		
	K_m	k_{cat}	k_{cat}/K_m	K_m	k_{cat}	k_{cat}/K_m
	(μM)	(s^{-1})	(s^{-1}/μM)	(μM)	(s^{-1})	(s^{-1}/μM)
Penicillin G	178±55	34±1.5	0.19	737±52	849±28	1.15
Ampicillin	193±63	139±5	0.72	297±43	253±13	0.85
Cefuroxime	17±2	6.5±0.3	0.38	27±3	75±6	2.78
Ceftizoxime	21±5	3.9±0.3	0.18	101±25	53±3	0.52
Meropenem	59±2	35±2	0.59	268±15	435±82	1.62

doi:10.1371/journal.pone.0082080.t001

Table 2. MICs (μg/ml) for *E.coli* BL21 (DE3) host strain harboring the wild-type NDM-1 and Y229W enzymes.

Enzymes harbored in *E.coli* BL21 (DE3)	Antibiotics (μg/ml)				
	Penicillin G	Ampicillin	Cefuroxime	Ceftizoxime	Meropenem
Wild-type NDM-1	>256	>256	256	64	16
Y229W mutant	256	128	128	8	8

doi:10.1371/journal.pone.0082080.t002

values of the final 4 ns insured the reliability and suitability of these MD trajectories for further analysis.

The root-mean-square fluctuation (RMSF) of Cα atoms was also calculated with respect to the starting structures (Fig. 3D). In the enzyme systems, Loop 2 was significantly more flexible in Y229W mutant than in NDM-1. As expected, Loop 1 was also found to be fluctuant in both systems, although the fluctuation was less different between wild-type NDM-1 and Y229W mutant.
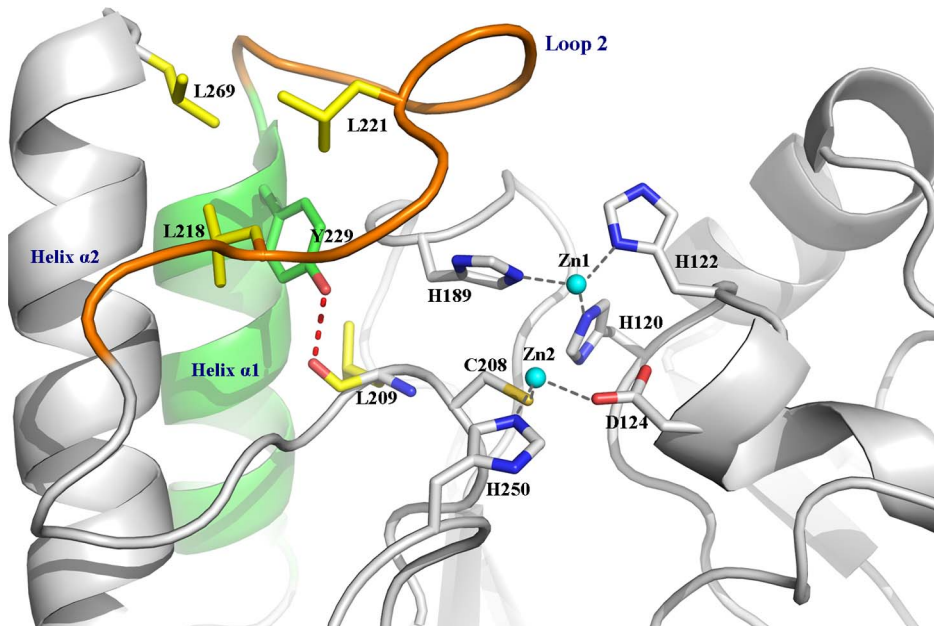
Distinct conformations of Loop 2 were obtained by clustering the MD trajectories of wild-type NDM-1 and Y229W mutant. The superimpositions of the conformations were shown in Fig. 3A and Fig. 3B. For both systems, the conformations superimposed well except in the flexible regions of Loop 1 and Loop 2. To facilitate substrate hydrolysis, the active site of the enzyme needs both stability and flexibility. Y229W mutation enhanced the flexibility of Loop 2, which could increase the kinetics of both substrate entrance (kon) and product egress (koff). This might be caused by the different steric and electrostatic characteristics between Trp and Tyr.

Hydrogen bond analyses of Loop 2. In order to investigate the reason of increased flexibility of Loop 2 after mutation, hydrogen bond analyses were performed for the last 4 ns of MD simulations. Hydrogen bonds were defined by a donor-acceptor distance of smaller than 3.5 Å and a donor-hydrogen-acceptor angle of larger than 120°. Overall, 13 hydrogen bonds existed in the Loop 2 (residues from 214 to 229) of wild-type NDM-1 and 10 hydrogen bonds existed in Y229W mutant (Table 3). The hydrogen bonds accepted by N220 in NDM-1 were not observed in Y229W mutant. In wild-type NDM-1, the occupancies of hydrogen bonds involving D225 were all above 99%, much larger than those in Y229W mutant. Such weaker hydrogen bonding interactions could contribute to the increased flexibility of Loop 2 in Y229W mutant. Moreover, T226 on Loop 2 of Y229W mutant formed hydrogen bonds with A230 on helix α1 and L269 on helix α2, facilitating the movement of Loop 2 away from Loop1, which resulted in an increased volume of the active site compared with that of wild-type NDM-1.

Interactions of NDM-1 and Y229W mutant with the hydrolyzed Ampicillin. To investigate the mutagenesis effect on the plasticity of protein and ligand binding, MD simulations of the enzyme-hydrolyzed Ampicillin complexes were performed. Both the wild-type NDM-1 and Y229W mutant systems reached equilibrated states after 16 ns. Compared with the apo-enzyme systems, the RMSDs of enzyme-product complexes were more stable for both wild-type NDM-1 and Y229W mutant (Fig. 4C). Although Loop 2 in Y229W mutant complex was still more fluctuant than that in wild-type NDM-1 complex, the RMSF values were much smaller for both systems (Fig. 4D), indicating the loop could be stabilized by interactions with the substrate molecules.

The last 4 ns of each MD trajectory was clustered based on heavy-atom RMSDs, and the central structure of the major cluster

Figure 2. The interactions around Y229 and the active site residues of NDM-1.
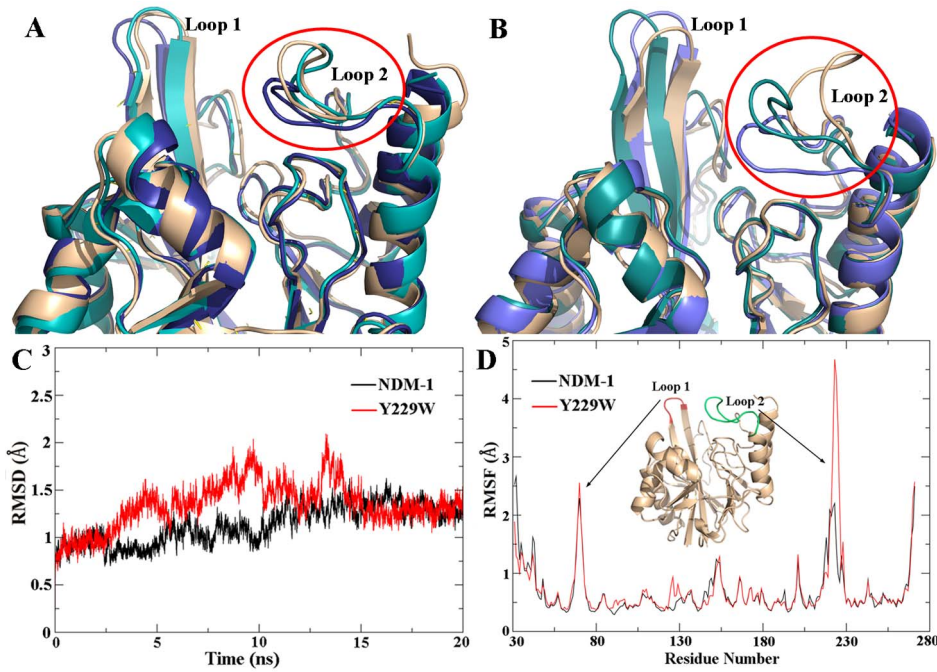doi:10.1371/journal.pone.0082080.g002

Figure 3. Distinct conformations of Loop 2 obtained by clustering the MD trajectory of the enzymes. (A) Superimposition of wild-type NDM-1; (B) Superimposition of Y229W mutant. (C) and (D) are the time evolution of the RMSDs and RMSFs of NDM-1 (black curve) and Y229W mutant (red curve) measured against the corresponding starting structures.
doi:10.1371/journal.pone.0082080.g003

Table 3. Hydrogen bonds existing in Loop 2 (residues from 214 to 229) of wild-type NDM-1 and Y229W mutant, and their occupancies during the last 4 ns of MD simulations.

NDM-1			Y229W mutant		
Donor	Acceptor	Occupancy (%)	Donor	Acceptor	Occupancy (%)
K214@ N	D212@OD1	84.14	K214@ N	D212@OD1	88.96
H261@ NE2	A215@O	90.19	H261@ NE2	A215@O	98.06
A215@ N	D212@O	99.55	A215@ N	D212@O	98.00
A224@ N	N220@O	99.76	——	——	——
D223@ N	N220@O	98.04	——	——	——
G222@ N	N220@OD1	85.64	——	——	——
——	——	——	W229@ N	D225@O	55.38
——	——	——	H228@ N	D225@O	53.72
E227@ N	D225@OD1	99.10	——	——	——
H228@ N	D225@OD1	99.43	——	——	——
D225@ N	G188@O	99.45	——	——	——
——	——	——	A230@ N	T226@O	85.96
——	——	——	T226@ OG1	L269@O	57.93
S232@ N	H228@O	96.63	S232@ N	H228@O	98.58
A231@ N	H228@O	60.30	——	——	——
Y229@ OH	L209@O	99.83	W229@ NE1	L209@O	98.75
A233@ N	Y229@O	93.83	A233@ N	W229@O	96.86

Only H-bonds with occupancies >50% are shown.
—— Not observed.
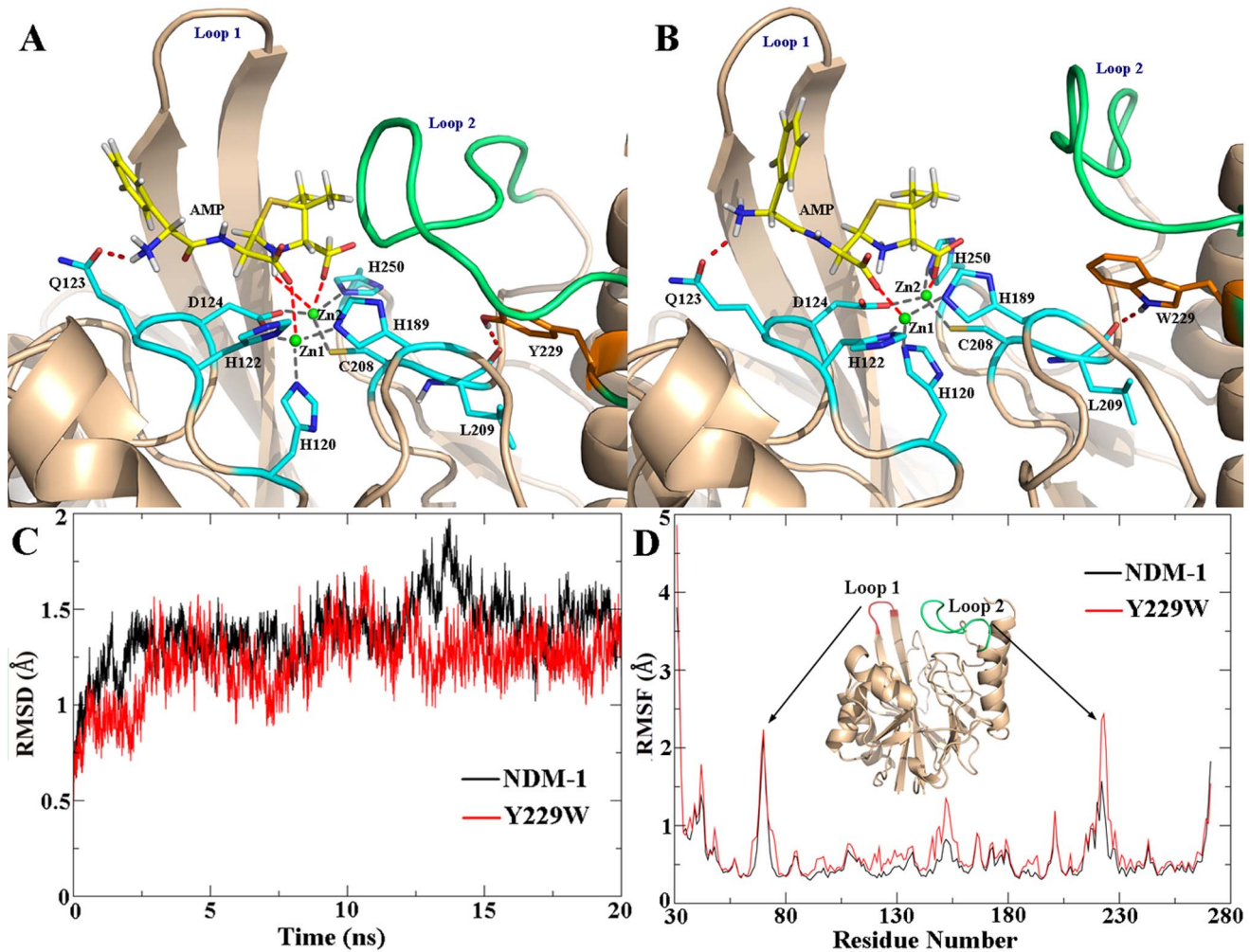doi:10.1371/journal.pone.0082080.t003

Figure 4. The central structure of the major cluster in the last 4 ns of (A) wild-type NDM-1 complexed with hydrolyzed Ampicillin, (B) Y229W mutant complexed with hydrolyzed Ampicillin. The time evolution of (C) RMSDs and (D) RMSFs of wild-type NDM-1 (black curve) and Y229W mutant (red curve), measured against the corresponding starting structures.
doi:10.1371/journal.pone.0082080.g004

(the member with the smallest average RMSD values to all other members of the major cluster) was extracted to serve as the representative structure of each MD simulation. The binding conformations of the representative structures (Fig. 4A and 4B) showed few changes in the active site in comparison with the crystal structure. Zn1 was coordinated by three histidine residues (H120, H122, and H189) and Zn2 was coordinated by D124, C208, and H250. The carboxylate group of the β-lactam ring coordinated to Zn2 through one oxygen atom and the newly formed carboxylate group after hydrolysis coordinated to Zn1. The nitrogen near the phenyl ring formed hydrogen bond with OE1 of Q123. The nitrogen atom of the β-lactam ring coordinated to Zn2 in the NDM-1 complex. However, this interaction was not present in the Y229W mutant complex. The hydrolyzed Ampicillin also formed hydrophobic interactions with Loop 1 and Loop 2, stabilizing both mobile loops.

Remarkably, the active-site cleft under Loop 1 and Loop 2 was broader in Y229W mutant (Fig. 5B) than that in wild-type NDM-1 (Fig. 5A). The enlarged binding groove of Y229W mutant can easily accommodate β-lactam antibiotics with different R groups. Besides, the hydrolyzed product could also exit from the binding groove faster thanks to less steric hindrance.

Binding free energy calculation. The binding free energy (MM/PBSA and MM/GBSA) of wild-type NDM-1/Y229W mutant with the hydrolyzed Ampicillin was calculated (Table 4). Both the MM/PBSA and MM/GBSA values suggested the hydrolyzed Ampicillin bound tighter to wild-type NDM-1 than to Y229W mutant, leading to an easier egress for the product of Y229W mutant. This correlates with the larger experimental k_{cat} values of Y229W mutant. These calculations also imply that the binding free energy of the original substrate with wild-type NDM-1 is greater than Y229W mutant as well, which is in conformity with our experimental K_m values. Thus, we propose that the product exiting and substrate entering might be the rate-limiting step in wild-type NDM-1- and Y229W-mediated β-lactams hydrolysis.

Discussion

NDM MβLs have gained a lot of attention owing to their broad hydrolytic spectrum on β-lactams and the current lack of effective β-lactamase inhibitors against NDM-carrying superbugs. In addition, continuous evolution of drug-resistant bacteria leads to the emergence of new NDM variants, which makes the situation
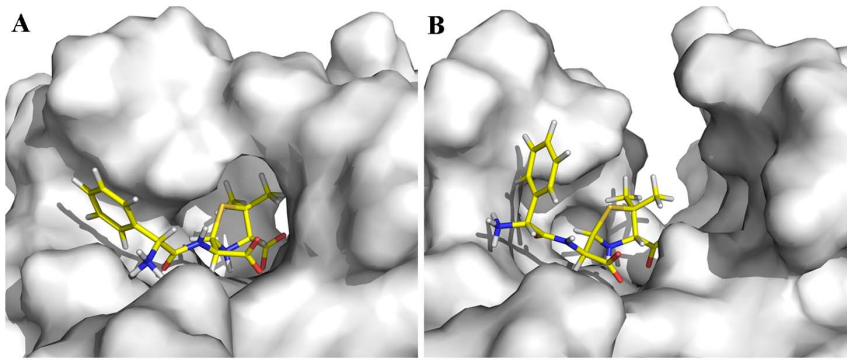
Figure 5. Surface representation of the central structure in the major cluster of the last 4 ns, showing the binding groove for substrates in (A) wild-type NDM-1, (B) Y229W mutant.
doi:10.1371/journal.pone.0082080.g005

more discouraging. To date, 9 NDM variants have been identified or assigned (http://www.lahey.org/Studies/other.asp#table1, data collected before June 25, 2013). Some variants obtained increased enzymatic activities by mutating only one or two remote amino acids, suggesting important roles of these non-active-site residues in the function of NDM MβLs. Numerous studies have been carried out to explore the substrate recognition and catalytic mechanism, and most of them focused on active-site residues such as D124, K211 and N220 [13,35].

Position 229 (244 in BBL numbering system) is very interesting since it may offer some evolutional clues of MβLs development. In most of the subclass B1 MβLs, a highly conserved Trp is observed, whereas in subclass B2/B3 MβLs, it is a Tyr. As we all know, most subclass B2/B3 MβLs exhibit narrower substrate spectrums than subclass B1 MβLs [2]. Unexpectedly, the broad-spectrum NDM-1 (subclass B1) employs a residue Tyr at position 229, which is usually conserved in B2/B3 MβLs. This prompted us to question whether the non-active-site substitution Y229W can influence the activity of NDM-1. Yu Guo *et al.* suggested that the peripheral residue Tyr229 may not directly participate in the enzymatic action of NDM-1, as confirmed by the minor effect of the Y229W mutation, but the conservation of this residue and its functional role in catalytic reaction in MBL superfamily should need further investigation [36]. Herein, we constructed the Y229W mutant of NDM-1 by site-directed mutagenesis and applied molecular dynamics simulations in order to investigate its effect on the structure and activity of NDM-1.

Biochemical analyses showed a simultaneous increase of K_m and k_{cat} upon Y229W mutation. For most of the tested antibiotics, the k_{cat} values exhibited larger increase than K_m, and thereby increased

the catalytic efficiency (k_{cat}/K_m) by 1~7 folds. However, *E coli.* carrying Y229W mutant showed reduced resistance to the tested antibiotics, which were inconsistent with the increased k_{cat}/K_m values. This might be caused by the decreased efficiency of mutant expression and culture conditions.

The non-active-site mutation Y229W may affect the catalytic efficiency via three different manners: 1) changing the kinetics of substrate entry or product exit by reducing or enlarging the volume of active-site pocket; 2) affecting the substrate binding by residue-residue interaction; 3) altering the stability of the three-dimensional (3D) structure [37]. To clarify this, MD simulations were performed to analyze the mutagenesis effect on Y229W mutant.

The substrate-enzyme interaction analysis (Fig. 4) revealed that the mutagenesis does not alter the catalytic properties of the enzyme. Superimposition of the conformations showed that Loop 2 is remarkably more flexible in Y229W mutant than that in wild-type NDM-1 (Fig. 3). The RMSF values also supported this point. The flexibility of Loop 2 in Y229W mutant might be caused by weaker interactions around the residues on Loop 2. For example, the number of hydrogen bonds around Loop 2 in Y229W mutant is less and some of the hydrogen bond occupancies are lower. In addition, the hydrophobic interactions between W229 and L221, L269 disappeared as their side chains deviated from the original direction.

Through strict computational means, the study of Freddie R. Salsbury Jr. *et al.* suggested that the flip of a loop indirectly involved in substrate binding can affect the catalytic efficiency and/or substrate specificity of an MBL while retaining a di-zinc active site [38]. Our study is in agreement with this point. We propose that the flexible Loop 2 could affect substrate entry and product exit by enlarging the active-site pocket as shown in the surface representation of substrate-enzyme complexes (Fig. 5). The broader active-site cleft under Loop 1 and Loop 2 in Y229W mutant can easily accommodate β-lactam antibiotics with different R groups and accelerate the egress of the hydrolyzed product, possibly contributing to increased k_{cat} values in Y229W mutant. Meanwhile, the larger active-site pocket could also decrease the binding energies (MM/PBSA and MM/GBSA) of the substrate with Y229W mutant, corresponding to the increased K_m values. Therefore, we propose that substrate-entry/product-release might be the rate-limiting step in a catalytic cycle.

Table 4. The binding free energies (hydrolyzed Ampicillin as the substrate) calculated by the MM-PBSA and MM-GBSA method.

Enzyme	Binding free energy model	ΔG_{gas}	ΔG_{solv}	ΔG
		(kcal/mol)	(kcal/mol)	(kcal/mol)
NDM-1	MM/PBSA	−124.82	96.77	−28.05
	MM/GBSA	−124.82	75.29	−49.53
Y229W	MM/PBSA	−72.29	57.51	−14.78
	MM/GBSA	−72.29	52.80	−19.49

doi:10.1371/journal.pone.0082080.t004

Conclusion

This study highlighted the importance of the non-active-site residue at position 229 in the evolution of NDM MβLs. The mutation from Tyr to Trp may not influence the overall structure of NDM-1, but it was shown herein to increase the flexibility of Loop 2 and broaden the binding pocket, which endowed the enzyme with increased turnover rates and decreased binding affinities. It is also implied that the Y229W mutant has higher structural flexibility near the active site than that of wild-type NDM-1, which probably broadens the substrate spectrum of the enzyme.

Author Contributions

Conceived and designed the experiments: JC HC HZ. Performed the experiments: HC FH. Analyzed the data: JC HC HZ XL. Contributed reagents/materials/analysis tools: XG WY. Wrote the paper: JC YS HZ.

References

1. Giamarellou H, Poulakou G (2009) Multidrug-resistant Gram-negative infections: what are the treatment options? Drugs 69: 1879–1901
2. Palzkill T (2013) Metallo-β-lactamase structure and function. Ann N Y Acad Sci 1277: 91–104
3. Park H, Brothers EN, Merz KM Jr (2005) Hybrid QM/MM and DFT investigations of the catalytic mechanism and inhibition of the dinuclear zinc metallo-β-lactamase CcrA from Bacteroides fragilis. J Am Chem Soc 127: 4232–4241
4. Perez-Llarena FJ, Bou G (2009) Beta-lactamase inhibitors: the story so far. Curr Med Chem 16: 3740–3765
5. Yong D, Toleman MA, Giske CG, Cho HS, Sundman K, et al. (2009) Characterization of a new metallo-beta-lactamase gene, bla(NDM-1), and a novel erythromycin esterase gene carried on a unique genetic structure in Klebsiella pneumonia sequence type 14 from India. Antimicrob Agents Chemother 53: 5046–5054
6. Kumarasamy KK, Toleman MA, Walsh TR, Bagaria J, Butt F, et al. (2010) Emergence of a new antibiotic resistance mechanism in India, Pakistan, and the UK: a molecular, biological, and epidemiological study. Lancet Infect Dis 10: 597–602
7. Hsu LY, Koh TH (2011) World Health Day 2011: combating antimicrobial resistance. Singapore Med J 52: 230–231
8. Bebrone C (2007) Metallo-beta-lactamases (classification, activity, genetic organization, structure, zinc coordination) and their superfamily. Biochem Pharmacol 74: 1686–1701
9. Brown NG, Horton LB, Huang W, Vongpunsawad S, Palzkill T (2011) Analysis of the functional contributions of Asn233 in metallo-β-lactamase IMP-1. Antimicrob Agents Chemother 55: 5696–5702
10. King DT, Worrall LJ, Gruninger R, Strynadka NC (2012) New Delhi metallo-β-lactamase: structural insights into β-lactam recognition and inhibition. J Am Chem Soc 134:11362–11365
11. Yang H, Aitha M, Hetrick AM, Richmond TK, Tierney DL, et al. (2012) Mechanistic and spectroscopic studies of metallo-β-lactamase NDM-1. Biochemistry 51: 3839–3847
12. Zhang HM, Hao Q (2011) Crystal structure of NDM-1 reveals a common β-lactam hydrolysis mechanism. FASEB J 25: 2574–2582
13. Kim Y, Cunningham MA, Mire J, Tesar C, Sacchettini J, et al. (2013) NDM-1, the ultimate promiscuous enzyme: substrate recognition and catalytic mechanism. FASEB J 27: 1917–1927
14. Hornsey M, Phee L, Wareham DW (2011) A novel variant, NDM-5, of the New Delhi metallo-β-lactamase in a multidrug-resistant Escherichia coli ST648 isolate recovered from a patient in the United Kingdom. Antimicrob Agents Chemother 55: 5952–5954
15. Nordmann P, Boulanger AE, Poirel L (2012) NDM-4 metallo-β-lactamase with increased carbapenemase activity from Escherichia coli. Antimicrob Agents Chemother 56: 2184–2186
16. Galleni M, Lamotte-Brasseur J, Rossolini GM, Spencer J, Dideberg O, et al. (2001) Standard numbering scheme for class B beta-lactamases. Antimicrob Agents Chemother 45: 660–663
17. Liang Z, Li L, Wang Y, Chen L, Kong X, et al. (2011) Molecular basis of NDM-1, a new antibiotic resistance determinant. PLoS One. doi:10.1371/journal.pone.0023606
18. Shen BZ, Yu Y, Chen H, Cao X, Lao X, et al. (2013) Inhibitor discovery of full-length New Delhi metallo-β-Lactamase-1 (NDM-1). PLoS One. doi:10.1371/journal.pone.0062955
19. Vanhove M, Zakhem M, Devreese B, Franceschini N, Anne C, et al. (2003) Role of Cys221 and Asn116 in the zinc-binding sites of the Aeromonas hydrophila metallo-beta-lactamase. Cell Mol Life Sci 60: 2501–2509
20. Laraki N, Franceschini N, Rossolini GM, Santucci P, Meunier C, et al. (1999) Biochemical characterization of the Pseudomonas aeruginosa 101/1477 metallo-β-lactamase IMP-1 produced by Escherichia coli. Antimicrob Agents Chemother 43: 902–906
21. Thomas PW, Zheng M, Wu S, Guo H, Liu D, et al. (2011) Characterization of purified New Delhi metallo-β-lactamase-1. Biochemistry 50: 10102–10113
22. Pang YP (1999) Novel zinc protein molecular dynamics simulations: Steps toward antiangiogenesis for cancer treatment. J Mol Model 5:196–202
23. Oelschlaeger P, Schmid RD, Pleiss J (2003) Insight into the mechanism of the IMP-1 metallo-beta-lactamase by molecular dynamics simulations. Protein Eng 16: 341–350
24. Oelschlaeger P, Schmid RD, Pleiss J (2003) Modeling domino effects in enzymes: Molecular basis of the substrate specificity of the bacterial metallo-beta- lactamases IMP-1 and IMP-6. Biochemistry 42: 8945–8956
25. Bayly CI, Cieplak P, Cornell WD, Kollman PA (1993) A well-behaved electrostatic potential based method using charge restraints for deriving atomic charges–the resp model. J Phys Chem 97: 10269–10280
26. Case DA, Darden TA, Cheatham TE III, Simmerling CL, Wanget J, et al. (2012) AMBER 12. University of California, San Francisco
27. Jorgensen WL, Chandrasekhar J, Madura JD, Impey RW, Klein ML (1983) Comparison of simple potential functions for simulating liquid water. Chem Phys 79: 926–935
28. Pastor RW, Brooks BR, Szabo A (1988) An analysis of the accuracy of Langevin and molecular dynamics algorithms. Mol Phys 65: 1409–1419
29. Darden T, York D, Pedersen L (1993) Particle mesh Ewald – an N. Log (N) method for Ewald sums in large systems. J Chem Phys 98: 10089–10092
30. Ryckaert JP, Ciccotti G, Berendsen HJC (1977) Numerical-integration of Cartesian equations of motion of a system with constraints–molecular dynamics of nalkanes. J Comput Phys 23: 327–341
31. Zhang H, Yao Y, Yang H, Wang X, Kang Z, et al. (2012) Molecular dynamics and free energy studies on the carboxypeptidases complexed with peptide/small molecular inhibitor: mechanism for drug resistance. Insect Biochem Mol Biol 42: 583–595
32. Chen H, Zhang Y, Li L, Han JG (2012) Probing ligand-binding modes and binding mechanisms of benzoxazole-based amide inhibitors with soluble epoxide hydrolase by molecular docking and molecular dynamics simulation. J Phys Chem B 116: 10219–10233
33. Gonzalez JM, Buschiazzo A, Vila AJ (2010) Evidence of adaptability in metal coordination geometry and active-site loop conformation among B1 metallo-beta-lactamases. Biochemistry 49: 7930–7938
34. Valdez CE, Sparta VM, Alexandrova NA (2013) The Role of the Flexible L43-S54 Protein Loop in the CcrA Metallo-β-lactamase in Binding Structurally Dissimilar β-Lactam Antibiotics. J Chem Theory Comput 9: 730–737
35. Zhu K, Lu J, Liang Z, Kong X, Ye F, et al. (2013) A quantum mechanics/molecular mechanics study on the hydrolysis mechanism of New Delhi metallo-β-lactamase-1. J Comput Aid Mol Des 27: 247–256
36. Guo Y, Wang J, Niu G, Shui W, Sun Y, et al. (2011) A structural view of the antibiotic degradation enzyme NDM-1 from a superbug. Protein Cell 2:384–394
37. Zhou H, Qu Y, Kong C, Shen E, Wang J, et al. (2013) The key role of a non-active-site residue Met148 on the catalytic efficiency of meta-cleavage product hydrolase BphD. Appl Microbiol Biot. doi: 10.1007/s00253-013-4814-0
38. Salsbury FR Jr, Crowder MW, Kingsmore SF, Huntley JJ (2009) Molecular dynamic simulations of the metallo-beta-lactamase from Bacteroides fragilis in the presence and absence of a tight-binding inhibitor. J Mol Model 15: 133–145